Theoretical study of resonant vibrational excitation of CO_2 by electron impact

T. N. Rescigno
Lawrence Berkeley National Laboratory, Computing Sciences, Berkeley, California 94720
and Lawrence Livermore National Laboratory, Physics and Advanced Technologies, Livermore, California 94551

W. A. Isaacs
Lawrence Livermore National Laboratory, Physics and Advanced Technologies, Livermore, California 94551

A. E. Orel
Department of Applied Science, University of California, Davis, California 95616

H.-D. Meyer
Universität Heidelberg, Im Neuenheimer Feld 229, D-69120 Heidelberg, Germany

C. W. McCurdy
Lawrence Berkeley National Laboratory, Computing Sciences, Berkeley, California 94720
and Department of Applied Science, University of California, Davis, California 95616
(Received 13 September 2001; published 20 February 2002)

We report the results of a fully *ab initio* study of resonant vibrational excitation of CO_2 by electron impact via the 3.8 eV $^2A_1$ shape resonance. First, we solve the fixed-nuclei, electronic scattering problem using the complex Kohn variational method for a variety of symmetric-stretch geometries and for a range of bending angles. We then carry out a three-mode treatment of the nuclear dynamics using a complex local potential or ''boomerang'' model using resonance parameters derived from our calculated fixed-nuclei cross sections. The results show that a multidimensional treatment of the nuclear motion is essential for a proper description of the vibrational dynamics of CO_2, in particular for describing resonant excitation of the two components of the well-known lowest Fermi dyad.

DOI: 10.1103/PhysRevA.65.032716 PACS number(s): 34.80.Gs

I. INTRODUCTION

Much of the work on *ab initio* treatments of electron-molecule collisions has been directed at developing accurate methods for solving the fixed-nuclei problem posed by electron scattering from a nonspherical, polarizable charge distribution, with full allowance for exchange. Of the many approaches that have been attempted over the past two decades, several have proved flexible and robust enough to be capable of treating elastic and inelastic collisions with fairly general multielectronic-state expansions and accurate target wave functions, even in the case of polyatomic targets [1]. While accurate *ab initio* calculations of low-energy electron-molecule scattering are now being performed even for mid-sized polyatomic targets, it is the case that the preponderance of these calculations have been carried out at a single fixed-nuclei geometry corresponding to the equilibrium target configuration. The fixed-nuclei electronic problem gives an important, but often incomplete, description of the full electron-molecule collision. The nuclear dynamics problem, i.e., the set of processes that control the flow of electronic energy into nuclear degrees of freedom, is also of fundamental importance in studying electron collisions with polyatomic targets and is key to developing an understanding of *electron-driven chemistries* in a variety of contexts, from modeling energy flow in a gas laser system to understanding the production of reactive species in low-temperature processing plasmas.

Negative ion shape resonances, which are ubiquitous in low-energy electron-polyatomic cross sections, play an important role in both vibrational excitation and dissociative electron attachment (DEA). The energy dependence of a resonance feature from a fixed-nuclei electronic cross section calculation can give only some indication of the probabilities of resonant vibrational excitation or DEA; determining the cross sections for such processes requires detailed study of the nuclear dynamics. The equations that govern the dynamics of the nuclei have been derived by applying formal resonance scattering theory [2] to electron-molecule collisions within a Born-Oppenheimer framework [3]. The formal theory is most often applied in an approximate form known as the local complex potential or ''boomerang'' model [4]. The one-dimensional version of this equation can easily be parametrized and has therefore become a popular and often successful semiempirical tool in the analysis of resonant electron-molecule cross sections.

The resonance parameters needed to construct a local complex potential for the boomerang model need not be treated as semiempirical parameters if they can be extracted from an analysis of the cross sections obtained from accurate fixed-nuclei scattering calculations [5]. Alternatively, one could attempt to compute the resonance parameters directly by analyzing the complex eigenvalues of a non-Hermitian (complex-symmetric) Hamiltonian obtained either by complex scaling [6,7] or by complex absorbing potential methods [8,9]. The viability of such an *ab initio* approach to the com-

plete problem has been demonstrated for a number of diatomic targets. The extension of the basic approach to polyatomic targets would require a complex potential energy *surface* and an appropriate extension of the dynamics calculations to include multiple nuclear degrees of freedom. In fact, very little work has been done in this area and the majority of the calculations that have appeared have used a one-dimensional treatment of the nuclear motion, even in the case of polyatomics. There have been a few notable exceptions. Using a completely *ab initio* approach, Orel and Kulander [10] have studied resonant dissociative recombination of H_3^+ with a two-dimensional treatment of the dynamics. More recently, Kazansky [11,12] has looked at the effects of coupling several vibronic modes in the case of resonant vibrational excitation of CO_2. These studies, however, employed model potential parameters.

In this paper, we undertake an *ab initio* study of resonant vibrational excitation of CO_2 by electron impact. CO_2 is interesting for a number of reasons. Although the principal features of the low-energy cross sections, namely, the dramatic rise in the total cross section below 2 eV and the resonance feature near 3.8 eV, have been the subject of many theoretical investigations, starting with the pioneering model potential calculations of Morrison, Lane, and Collins [13], it was not until 1998 that an *ab initio* study was performed that was able to show conclusively that the low-energy rise in the elastic cross section was the result of a virtual state [14]. Only recently has *ab initio* theory correctly accounted for both the low-energy behavior and the resonance peak [15,16] or been able to achieve quantitatively correct differential cross sections below 6 eV [15].

There have been a number of experimental studies of resonant vibrational excitation of CO_2. Oscillatory structure in the cross section over the resonance region was first revealed in transmission experiments by Bonness and Hasted [17]. More observations followed and detailed studies of vibrational excitation were performed by Cadez *et al.*, [18] who measured differential excitation functions at several fixed angles and noted that the resonance couples strongly to symmetric-stretch motion, having observed energy-loss spectra at 4 eV for the symmetric-stretch mode up to $\nu' = 25$. These authors also observed some structure in the excitation functions which became more pronounced with increasing vibrational quantum number. Cadez *et al.* [18] also performed one-dimensional boomerang calculations with potential parameters chosen to give a best fit to the observed data. Currell and Comer [19] cited evidence for strong polyatomic effects in the excitation functions of certain vibrational levels, in particular the (1,0,0) and (0,2,0) modes, which are strongly coupled members of a resonant Fermi dyad. They argued that bending as well as stretching deformations of the resonance state both played a role in the excitation dynamics. This assertion was given further support by the measurements of Johnstone, Akther, and Newell [20], who reported absolute cross sections for individual vibrational levels by recording several electron energy-loss spectra over a range of incident energies. The energy resolution of the experiment did not permit observation of the peaks for individual members of the Fermi polyads, so a least squares fitting procedure was used in analyzing the data. Most recently, Allan [21] has been able to achieve a decisive improvement in energy resolution down to 7 meV which allowed him to perform separate measurements of the excitation functions for each member of the lowest Fermi dyad and to measure the excitation cross sections with high accuracy. The fact that modern *ab initio* methods have now been shown to be capable of achieving a high level of accuracy in solving the fixed-nuclei problem for this system and that experimental results of unprecedented quality are now available has prompted us to undertake a detailed first-principles study of the vibrational excitation dynamics in the $e^- + CO_2$ system. We are presenting our initial results of that study in this paper.

The outline of this paper is as follows. The next section gives a brief description of the local complex potential or boomerang model for resonant vibrational excitation. The equations are then recast in time-dependent form. We follow with a brief discussion of methods for solving the time-dependent Schrödinger equation and describe the multiconfiguration time-dependent Hartree method used in this work. Our results for CO_2 are presented in Sec. III. We begin with a brief discussion of the fixed-nuclei calculations from which the complex resonance surface was constructed, and then present the results of our multidimensional complex local potential calculations. Section IV contains a discussion and some concluding remarks. We employ atomic units throughout.

II. THEORETICAL FORMULATION

Theoretical treatments of resonant vibrational excitation are generally based on rigorous resonance scattering theory [3], formulated within the Born-Oppenheimer approximation. The principal result of the theory is the so-called nuclear wave equation that governs the nuclear dynamics due to the resonance state(s):

$$[E - E_{res} - K_s]\xi_{\nu_i}(s) = (\psi_{res} H_{el} P \phi_{\nu_i}) + (\psi_{res} H_{el} P G_P^+ P H_{el} \psi_{res}) \xi_{\nu_i}(s), \tag{2.1}$$

where E is the total energy, K_s is the nuclear kinetic energy operator, H_{el} is the fixed-nuclei electronic Hamiltonian, ψ_{res} is the electronic resonance wave function, E_{res} is the ''adiabatic'' resonance energy $\langle \psi_{res} | H_{el} | \psi_{res} \rangle$, and $P\phi_{\nu_i}$ is the nonresonant background scattering wave function associated with an initial target state labeled by ν_i. The variable s is used to denote the internal nuclear coordinates. This is an inhomogeneous wave equation which, due to the presence of the nuclear Greens's function G_P^+, involves an effective Hamiltonian that is complex, nonlocal, and energy dependent. While explicit construction of the effective Hamiltonian from first principles is possible [22], the computational effort required for a realistic calculation on a polyatomic target would be extremely tedious, and hence we follow the usual practice of approximating the effective nuclear Hamiltonian by a simpler local operator.

A. Local complex potential model

The complex local potential or boomerang model can be derived from the nuclear wave equation under a set of simplifying approximations. The conditions under which these approximations are justified are well understood [5] and, in a few cases, have been tested against the rigorous nonlocal theory [23–25]. The boomerang model for the wave equation that determines the nuclear dynamics is [4]

$$[E-K_s-E_{res}(s)+i\Gamma(s)/2]\xi_\nu(s)=\phi_\nu(s). \tag{2.2}$$

In Eq. (2.2), the negative ion energy surface is characterized by a real part $E_{res}(s)$ and an imaginary part $-i\Gamma(s)/2$, and the ''entry amplitude'' ϕ_ν is defined as

$$\phi_\nu(s)=[\Gamma(s)/2\pi]^{1/2}\eta_\nu(s), \tag{2.3}$$

where η_ν is the initial vibrational wave function of a neutral target. The resonant T matrix for vibrational excitation is obtained by projecting the solution of Eq. (2.2) onto the ''exit amplitude'' $\phi_{\nu'}$:

$$T_{\nu\nu'}(E)=\langle\phi_{\nu'}|\xi_\nu\rangle. \tag{2.4}$$

Combining Eqs. (2.2) and (2.4) allows us to write $T_{\nu\nu'}(E)$ as the matrix element of a nuclear Green's function between entry and exit amplitudes:

$$T_{\nu\nu'}(E)=\langle\phi_{\nu'}|\frac{1}{E-K_s-E_{res}(s)+i\Gamma(s)/2}|\phi_\nu\rangle. \tag{2.5}$$

B. Time-dependent Schrödinger equation

The differential equations of the boomerang model may be recast in a time-dependent formulation, as first shown by McCurdy and Turner [26], by writing the nuclear Green's function in Eq. (2.5) as the Fourier transform of the propagator for the time-dependent Schrödinger equation. The resonant T matrix for vibrational excitation is then expressed as

$$T_{\nu\nu'}(E)=-i\int_0^\infty dt e^{iEt}\langle\phi_{\nu'}|\Psi_t\rangle, \tag{2.6}$$

with

$$\Psi_t=e^{-iHt}\phi_\nu \tag{2.7}$$

and

$$H=K_s+E_{res}(s)-i\Gamma(s)/2. \tag{2.8}$$

The physical content of the boomerang model is that the electron is first captured into a temporary negative ion state with a probability determined by the entry amplitude. The nuclear Green's function controls the evolution of the negative ion state and the probability of vibrational excitation is determined by an overlap with the exit amplitude. In the time-dependent picture, the meaning of Eqs. (2.6)–(2.8) is clear: the resonant transition amplitude for excitation is given as the Fourier transform of the overlap between a wave packet propagating on a complex potential surface and a stationary packet determined by the final state. Since the potential surface is complex, the normalization of the wave packet Ψ_t in Eq. (2.7) is not conserved, and the packet decays as a function of time at a rate determined by the magnitude of the resonance width.

For problems with only one nuclear degree of freedom, there are no obvious computational advantages in choosing the time-dependent approach over the time-independent approach other than for the physical insight it offers into the problem. However, for problems with multiple degrees of freedom, there are decided advantages to the time-dependent approach, since it does not involve the solution of large systems of complex linear equations. Moreover, the exponential decay of the wave packet generally leads to its effective disappearance after only a few vibrational periods, so the wave packet need only be propagated for a short time. The time-dependent approach can thus be made quite efficient, as we shall see, even for multidimensional problems.

The ''standard'' method for solving the time-dependent Schrödinger equation proceeds by introducing a discrete set of points for each degree of freedom and constructing an explicit solution of the equations of motion for a wave packet propagating in time on the discrete, multidimensional grid. A serious problem with this approach is that the computational effort required scales exponentially with the number of degrees of freedom, making it prohibitively expensive to implement as the number of degrees of freedom grows. Several approximate methods have been developed to remove this obstacle. In the time-dependent Hartree (TDH) method, for example, the wave function is represented as a single product of one-dimensional functions, thereby simplifying the computational effort at the cost of a proper treatment of correlation between the degrees of freedom. The multiconfiguration time-dependent Hartree (MDTDH) method [27] offers a practical alternative to the TDH method that retains the essential rigor of the standard method. In the MCTDH method, as in the standard method, we start with a time-independent orthonormal product basis set:

$$\{\chi^{(1)}_{j_1}(Q_1)\cdots\chi^{(f)}_{j_f}(Q_f)\},\quad j_i=1,\ldots,N_i, \tag{2.9}$$

where we have assumed that there are f degrees of freedom in a problem described by nuclear coordinates $Q_1,\ldots,Q_f$. For computational efficiency, the basis functions $\chi^{(i)}_{j_i}$ are chosen as the basis functions of a discrete variable representation (DVR) [28].

The central idea in the MCTDH scheme is that one can employ a smaller, but now time-dependent, basis for expanding the wave function, i.e.,

$$\Psi(Q_1,\ldots,Q_f,t)=\sum_{j_1=1}^{n_1}\cdots\sum_{j_f=1}^{n_f}A_{j_1\cdots j_f}(t)\prod_{k=1}^{f}\varphi^{(k)}_{j_k}(Q_k,t), \tag{2.10}$$

with $n_k\ll N_k$. The single-particle functions in turn are represented as linear combinations of the primitive basis in Eq. (2.9),

$$\varphi_{j_k}^{(k)}(Q_k,t)=\sum_{i_k=1}^{N_k} c_{i_k j_k}^{(k)}(t)\chi_{i_k}^{(k)}(Q_k). \tag{2.11}$$

Since both the coefficients $A_{j_1\cdots j_f}$, and the single-particle functions are time dependent, the wave function representation is not unique. Uniqueness can be achieved by imposing additional constraints on the single-particle functions which keep them orthonormal for all times [27]. The MCTDH method has been applied to a variety of problems ranging from reactive and surface scattering to the determination of photodissociation and photoabsorption spectra (see [27] and references therein). The MCTDH approach is particularly useful when treating large systems. An impressive success of the MCTDH method was the calculation of the absorption spectrum of the pyrazine molecule [29,30] in which the quantal motion of all 24 internal degrees of freedom evolving on two coupled electronic surfaces was accurately determined. Due to the existence of a conical intersection in this system, all modes are coupled, giving raise to highly complex motion. More recently, the MCTDH method has been applied to the spin-boson model including 80 vibrational modes [31].

In our calculations on CO_2, we have tested the accuracy of the MCTDH scheme by carrying out boomerang calculations in both one and two dimensions (1D and 2D) using both the standard method and the MCTDH method. The two methods produced virtually identical results for this problem. For the 3D calculations, we used only the MCTDH method.

III. COMPUTATIONS

To recapitulate briefly, the procedure we followed for computing the e^-+CO_2 vibrational excitation cross sections begins with a variational determination of the fixed-nuclei electron scattering cross sections, for the appropriate total symmetry, at a series of different nuclear geometries. From each such calculation, we obtain a resonance energy and width by examining the energy dependence of the eigenphase sum [32]. If the geometry is such that the CO_2^- ion is electronically bound, then the eigenphase sum will show no evidence of a resonance. For these geometries, the width $\Gamma(s)$ is taken to be zero and $E_{res}(s)$ is obtained from the lowest eigenvalue of the $(N+1)$-electron electronic Hamiltonian. From the electronic resonance parameters, we construct an analytic expression for the complex resonance surface from a least squares fit of the computed fixed-nuclei resonance energy data.

For solving the time-dependent Schrödinger equation, we use conventional normal coordinates [33], with the restriction that the two CO bond distances are constrained to be equal. With this restriction, the symmetric-stretch coordinate S_1 and the doubly degenerate bend coordinates S_{2a} and S_{2b} become

$$S_1=2R\cos\theta, \tag{3.1}$$

$$S_{2a}^2+S_{2b}^2=R^2\sin^2\theta/[1+M_C/(2M_O)]^2, \tag{3.2}$$

where R is the CO bond distance and θ measures the angle of one of the CO bonds from linear geometry. The reduced masses in these coordinates are

$$\mu_1=M_O/2, \tag{3.3}$$

$$\mu_{2a}=\mu_{2b}=M_C\left(1+\frac{M_C}{2M_O}\right). \tag{3.4}$$

We have performed calculations in one, two, and three-dimensions. For the 1D calculations, we use only the symmetric-stretch coordinate. For the 2D calculations, we use only one of the degenerate bending modes, thereby restricting the nuclei to motion in a fixed plane.

A. Resonance surface construction

The fixed-nuclei calculations were carried out using the complex Kohn variational method, as described in our earlier paper [15]. In the Kohn method, we use a stationary principle for the T matrix,

$$T_{stat}=T_{trial}-2\int \Psi(H-E)\Psi, \tag{3.5}$$

which is evaluated with a trial wave function for the $(N+1)$-electron system of the form

$$\Psi=\mathcal{A}[\Phi_o(\vec{r}_1,\ldots,\vec{r}_N)F(\vec{r}_{N+1})]+\sum_\mu d_\mu\Theta_\mu(\vec{r}_1,\ldots,\vec{r}_{N+1}), \tag{3.6}$$

where Φ_o is the (Hartree-Fock) ground state of CO_2, $\mathcal{A}$ antisymmetrizes the coordinates of the incident electron with those of the target electrons, and the sum contains square-integrable, $(N+1)$-electron terms that describe correlation and polarization effects. The scattering function $F(\vec{r}_{N+1})$ is further expanded in a combined basis of Gaussian (ϕ_i) and continuum (Ricatti-Bessel, j_l, and Hankel h_l^+) basis functions

$$F(\vec{r})=\sum_i c_i\phi_i(\vec{r})+\sum_{lm}[j_l(kr)\delta_{ll_o}\delta_{mm_o}+T_{ll_omm_o}h_l^+(kr)]Y_{lm}(\hat{r})/r. \tag{3.7}$$

Applying the stationary principle [Eq. (3.5)] results in a set of linear equations for the coefficients c_i, d_μ, and $T_{ll_omm_o}$. The T-matrix elements $T_{ll_omm_o}$ are the fundamental dynamical quantities from which all fixed-nuclei cross sections are derived.

Calculated resonance positions and lifetimes are critically sensitive to a proper description of the dynamic response of the target to the incident electron, an effect that is described by including asymptotically decaying closed channels in the trial wave function. These terms are chosen by singly exciting the occupied target orbitals into unoccupied virtual orbitals. For symmetries in which shape resonances appear, we

have found that a ''relaxed self-consistent field'' procedure, which includes only symmetry- and spin-conserving single excitations of the target, captures the dominant physical effect of a shape resonance, which is relaxation of the target in the presence of an extra electron. These procedures, along with other parameters of the calculations, are fully described in Ref. [15]. In that earlier work, we carried out calculations in $^2\Pi_u$ symmetry for several different linear, symmetric-stretch geometries. For this work, we have extended those calculations to include bent geometries as well, using the same basis sets and prescriptions previously employed. Upon bending, the doubly degenerate $^2\Pi_u$ resonance state splits into two nondegenerate (Renner-Teller) states of symmetry $^2A_1$ and $^2B_1$. For the work reported here, we considered only the (lower) $^2A_1$ resonance surface.

Figure 1 gives a representative sampling of the fixed-nuclei $^2\Pi_u(^2A_1)$ cross sections for linear and bent geometries. Figure 1(a) shows that, as the molecule is stretched from its equilibrium position, the resonance energy drops and its width decreases. In linear geometry, the $^2\Pi_u$ resonance state crosses the neutral ground state, i.e., becomes electronically bound, at a CO distance of ~ 2.55 bohr. Figure 1(b) shows the effect of bending the molecule while holding the CO bond lengths fixed at their equilibrium values (2.194 bohr). For CO bond distances less than 2.5 bohr, bending the molecule away from linear geometry causes the resonance to broaden dramatically as it decreases in energy. The parameters extracted from these fixed-nuclei cross sections give the resonance energy relative to the CO_2 ground state. The total electronic energy is the resonance energy plus the CO_2 ground state energy. From a series of results such as these, we have constructed the energy and width surfaces for the CO_2^- ion shown in Fig. 2.

There are several points to be noted when considering these results. It is well known [34,35] that the $^2A_1$ state of CO_2^- is a stable negative ion, i.e., is electronically bound, when the molecule is either stretched or bent sufficiently. This behavior is reflected in the resonance width shown in Fig. 2, which goes to zero at such geometries. Stretching the molecule in linear geometry causes the width to decrease monotonically and the corresponding resonance parameters can easily be obtained by fitting the calculated eigenphase sums to a Breit-Wigner form with a smooth background. Calculating resonance parameters for large bending angles, however, presents something of a problem. Figure 1(b) shows that the resonance width increases as its position decreases, i.e., that the width remains finite as the resonance position approaches zero. To understand this behavior, it is important to bear in mind that symmetric-stretch motion with zero bend angle does not change the symmetry of the molecule and hence does not significantly change the angular momentum character of the resonance, whose lowest l component at equilibrium is p wave. Bending the molecule, however, breaks the degeneracy of the $^2\Pi_u$ resonance and mixes an s-wave component into the $^2A_1$ resonance. There is no angular momentum barrier associated with an s wave so it is not surprising that such an admixture causes the width, which is the inverse of the resonance lifetime, to increase.

The dramatically different properties of the resonance surface under stretching and bending reflect the fact that, mathematically, the trajectory of an s-wave resonance pole in the complex plane near zero energy is markedly different from that of a resonance that has angular momentum greater than zero. When plotted in the momentum plane, an s-wave pole approaches the origin from the negative imaginary axis, i.e., it becomes a virtual state. This means that at some point the real part of the resonance energy becomes negative or, equivalently, the magnitude of the imaginary part of the resonance momentum is larger than its real part. This behavior is illustrated in Fig. 3, in which a cut through the energy and width surfaces of Fig. 2 at a fixed CO bond length (2.4 bohr)

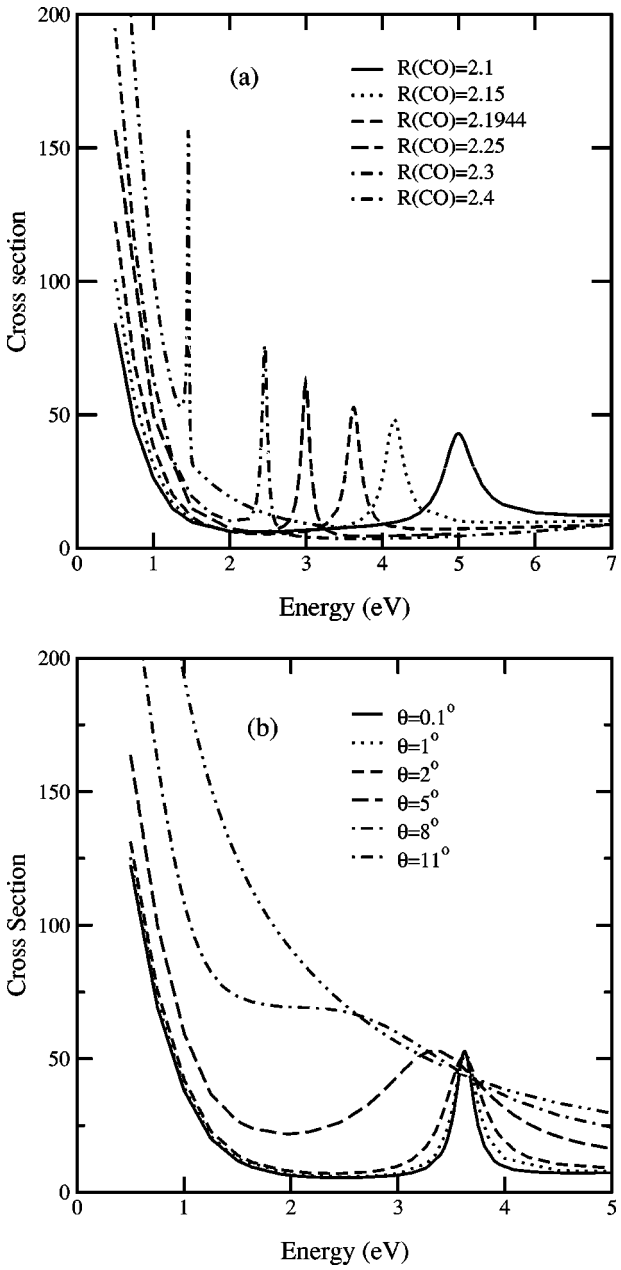

FIG. 1. $e^- + CO_2$ fixed-nuclei integrated cross sections, in units of a_0^2, in $^2A_1$ symmetry: (a) symmetric-stretch dependence in linear geometry; (b) bend-angle dependence at equilibrium CO bond distance.

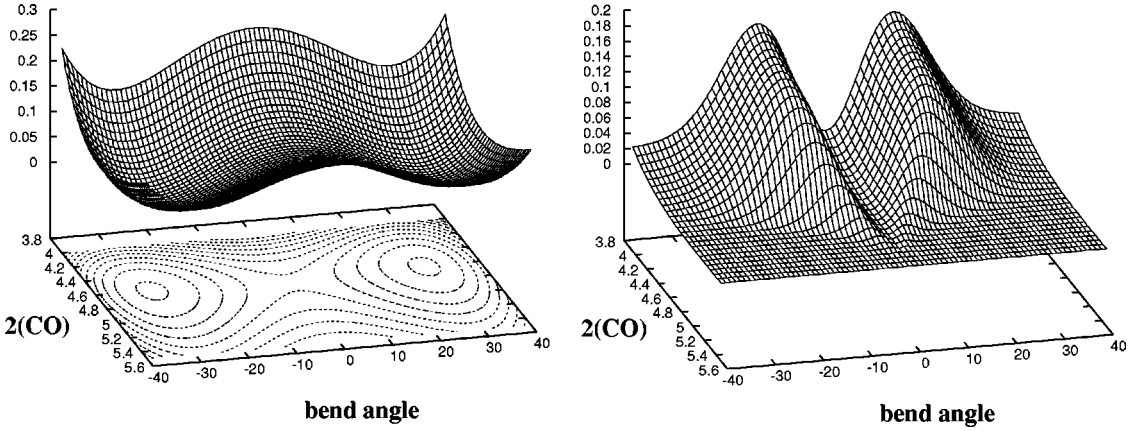

FIG. 2. Complex $^2A_1$ resonance energy of CO_2^-, in units of hartrees, as a function of symmetric-stretch distance, in units of bohrs, and bend angle, in degrees. Left panel shows the real part of the energy surface and the right panel shows the corresponding width.

is plotted as a trajectory in the complex energy and momentum planes. If the real part of the resonance energy is negative, it becomes ''invisible'' in the sense that it has no effect that can be seen in the energy dependence of the cross section. The practical consequence of this behavior in the case of the $^2A_1$ CO_2^- resonance is that there is a finite range of bending angles, from the point where the real part of the resonance energy first becomes negative to the point where it becomes electronically bound, where the resonance parameters cannot be extracted by analyzing the energy dependence of the fixed-nuclei cross sections. These portions of the resonance surfaces shown in Fig. 2, generally corresponding to bend angles between 15° and 30°, were therefore constructed by smoothly interpolating between the last points for which a Breit-Wigner fit of the data could be carried out and the points where the $^2A_1$ state becomes electronically bound. In fact, the vibrational excitation cross sections we calculated were rather insensitive to the portions of the resonance surface that had to be interpolated, since the wave packet rapidly decays as the width increases and hence hardly samples these large-angle regions.

Another point worth noting concerning the behavior of the resonance state with changing geometry is that the dipole moment of the CO_2 becomes nonzero when the molecule is nonlinear. That is another aspect of the symmetry breaking and the coupling of *s*-wave components into the resonance state that contributes to the increase in width with increasing bending angle. For small bending angles the dipole moment is small, and its consequences are not great. As the bending angle increases and the resonance surface crosses that of the ground state and becomes the bound anion, there might be another effect due primarily to the dipole. The long-range dipole potential can alter the nature of the transition of bound states to resonances and produce pole trajectories that are different from that shown in Fig. 3. That fact has been discussed by Domcke [22] in the context of electron scattering from heteronuclear diatomics. Ultimately, similar considerations may apply to the potential surfaces for CO_2^-, although the picture is substantially more complicated for polyatomics because there are multiple paths from one geometry to another. However, as we will see below, the wave

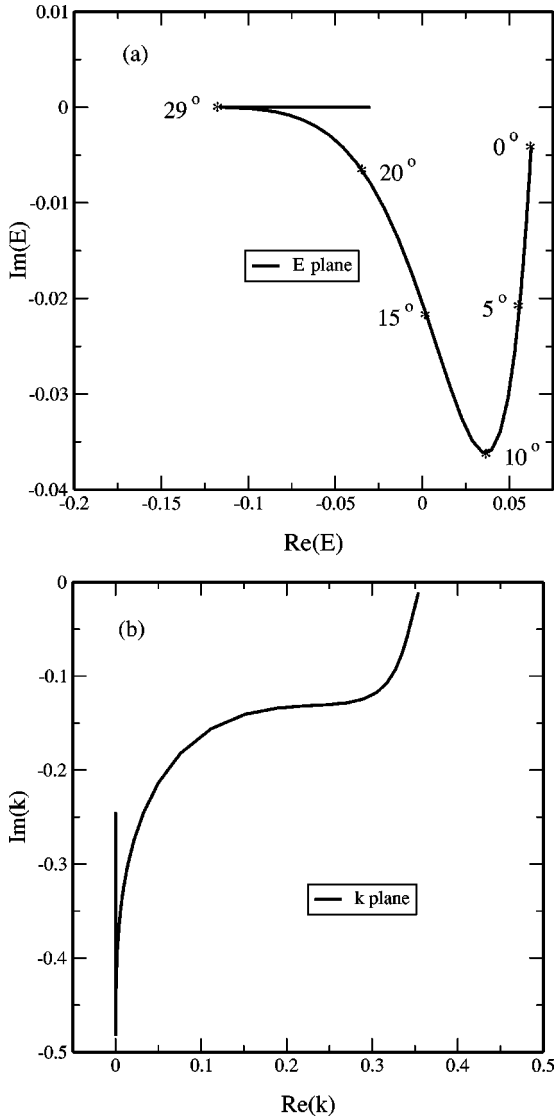

FIG. 3. Trajectory of the $^2A_1$ resonance pole as a function of bend angle for a fixed CO bond length (2.4 bohr). (a) Energy plane; several values of the bend angle are indicated along the curve. (b) Momentum plane. All scales are in atomic hartree units.

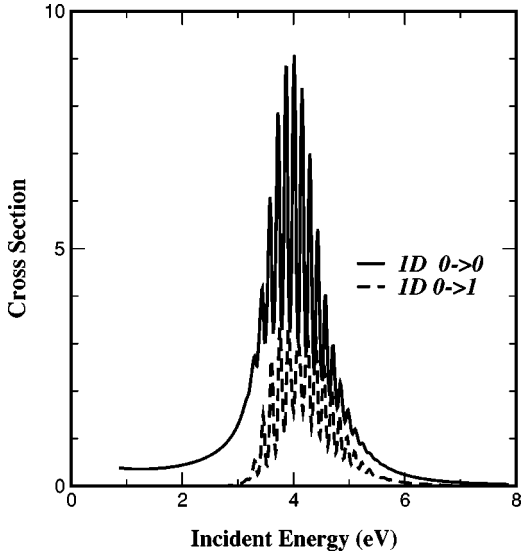

FIG. 4. One-dimensional (symmetric-stretch) boomerang results for e-CO_2 elastic ($0\rightarrow0$) and vibrationally inelastic ($0\rightarrow1$) cross sections, in units of a_0^2.

packet dynamics in the bending mode are such that for the calculations presented here the packet does not probe the crossing region significantly. Instead the region where the width is still increasing with increasing bending angle strongly determines the properties of the cross sections.

B. One-dimensional results

We first computed cross sections for symmetric-stretch excitation using a one-dimensional boomerang treatment that constrains the nuclei to lie along a line. Cadez *et al.* [18] had previously carried out such calculations, using semiempirically determined resonance parameters chosen to give a best fit to their measured cross sections. Figure 4 shows our 1D results for the resonant elastic and $0\rightarrow1$ vibrational excitation cross sections. The results at this level give something of a textbook picture of a ''diatomic'' shape resonance, similar to what is found in e^-+N_2 scattering, with deep, well-defined interference structures [4]. Experiment [18,20], however, shows structure that is far less pronounced than what these 1D results exhibit, with very shallow valleys between adjacent peaks. That Cadez *et al.* [18] were able to produce so little structure with their model calculations can be understood by comparing their empirically determined resonance parameters with our calculated results, which are both shown in Fig. 5. The real part of the resonance curve they derived is very close to our *ab initio* result, which is not surprising, since this parameter determines the position and overall envelope of the cross section. The width function they derived, however, is significantly larger than our result in the critical regions that the wave packet samples. This comparison serves to highlight the limitations of a 1D treatment for this target molecule: in order to successfully model the observed data, one is forced to compensate for the constrained linear motion by adopting what we believe to be an unrealistically

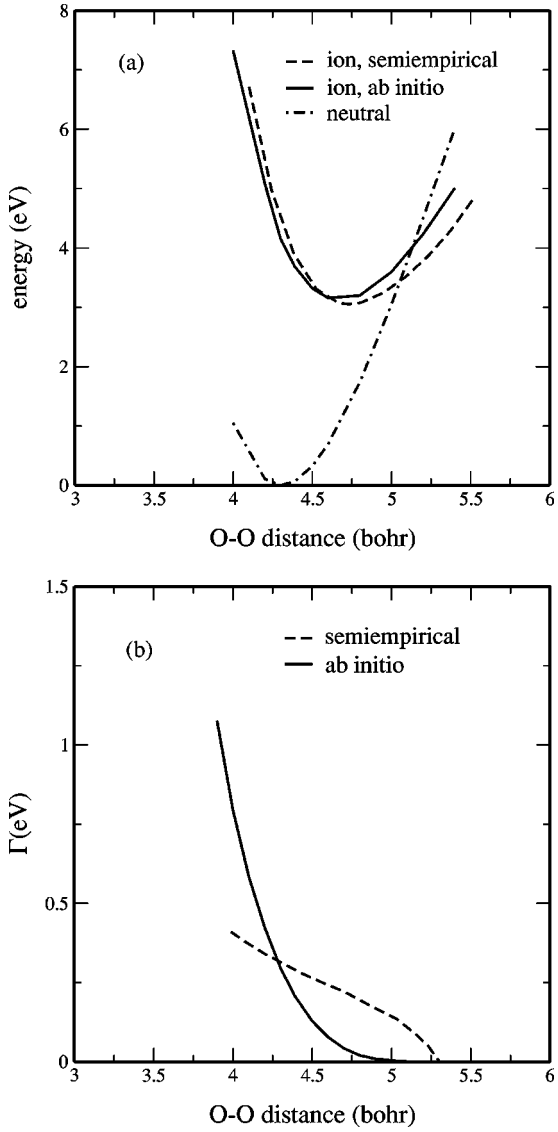

FIG. 5. Comparison of present *ab initio* resonance parameters for CO_2^- in linear geometry with semiempirical results of Cadez *et al.* [18] (a) CO_2 ground state and real part of CO_2^- resonance state. (b) CO_2 resonance width.

large value for the resonance width. This finding provided much of the impetus for the multidimensional studies presented in the next section.

C. Multidimensional results

To establish convergence criteria for the time-dependent calculations and to test the sensitivity of the results to parameters such as grid size, propagation time, and initial vibrational state representation, we first performed a series of coplanar, 2D calculations using both the MCTDH method and an explicit 2D wave packet propagation code that used a Chebyshev expansion of the propagator. For the MCTDH calculations, the ground vibrational state was obtained numerically on the grid by a relaxation technique, i.e., by propagating an initial wave packet in imaginary time. For the calculations with the explicit propagator, the ground vibra-

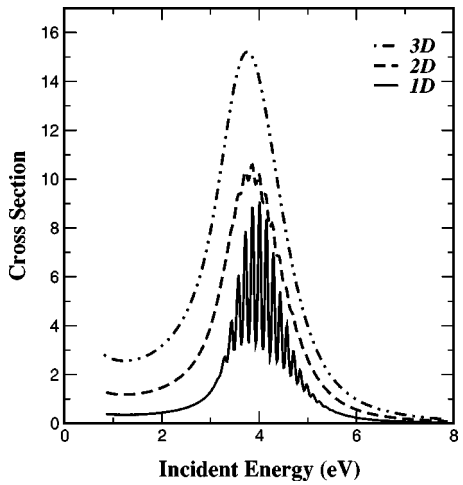

FIG. 6. Comparison of MCTDH results in 1D, 2D, and 3D for the resonant component of the vibrationally elastic e-CO_2 cross section, in units of a_0^2.

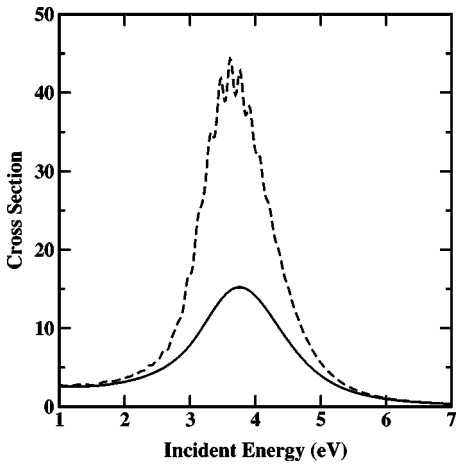

FIG. 7. Comparison of results for the vibrationally elastic cross section, in units of a_0^2, with the *ab initio* bending potential (solid curve) and with a width that decreases with increasing bending angle (broken curve).

tional state was approximated as a product of single-mode functions in the appropriate normal mode coordinates. The results were found to be completely insensitive to the representation of η_{ν_o} and we found virtually identical results with both approaches. In both cases, we used products of single-mode wave functions for the final target vibrational states.

For the 3D calculations, all of our results were obtained using the MCTDH method. The grids used covered the range $3.6 \leqslant S_1 \leqslant 6.0$ and $-1.5 \leqslant (S_{2a}, S_{2b}) \leqslant 1.5$. The DVR's used were a 64-point sine DVR in the symmetric stretch and a 64-point harmonic oscillator DVR in each of the bends. There were four single-particle functions in each dimension. The Fourier transform in Eq. (2.6) converged in all cases for times less than 75 atomic time units.

We begin with results for the resonant component of the elastic cross section. The 1D, 2D, and 3D results are shown in Fig. 6. We see that the pronounced interference features found in the 1D calculations are strongly damped in 2D and that in the 3D calculations they are entirely absent. This is the result of the sharp rise in the resonance width that accompanies bending, which in turn leads to an increasingly rapid decay of the wave packet. In the 1D model, the center of the wave packet can effectively survive long enough to reflect off the outer classical turning point on the potential wall and return with sufficient amplitude to produce the observed structure. When the bending degrees of freedom are introduced, the wave packet is rapidly damped. To verify that the effective absence of interference structure is indeed due to the functional dependence of the width on the bending motion, and not simply on the increased dimensionality of the resonance surface on which the wave packet propagates, we repeated the 3D calculations with a width function that has the same dependence on S_1, but *decreases* with increasing bend angle. Those results are shown in Fig. 7. The interference structure appears once again in these calculations. Figure 8 contrasts the behavior of the wave packets in 3D for the cases with and without the full bend-dependent width by showing a series of snapshots of the reduced density $\int |\Psi_t(S_1, S_{2a}, S_{2b})|^2 dS_{2b}$. It can be seen that on the $^2A_1$ surface Ψ_t effectively vanishes before it returns back to its initial position.

The boomerang model describes only the resonance component of the scattering; for the vibrationally elastic cross section, there will be a substantial nonresonant background component that must be included before a meaningful comparison with experiment can be made. We have therefore added a linear background, which we estimated from our earlier adiabatic nuclei calculations [15], to the 3D MCTDH results for the vibrationally elastic cross section. These results are shown in Fig. 9, along with three sets of experimental measurements [20,36,37]. Tanaka *et al.* [36] and Gibson *et al.* [37] report absolute integrated cross sections with which we can compare directly. Johnstone *et al.* [20] report absolute cross sections at a fixed scattering angle of 20°, so we have scaled their results by an overall constant, on the assumption that the angular dependence of the cross section is independent of energy [38]. The calculated results appear to be in better agreement with the results of Tanaka *et al.* and Johnstone *et al.* than with the measurements of Gibson *et al.*

Before turning our attention to the vibrationally inelastic results, we must make some preliminary remarks. Because the ground-state potential surface of CO_2 is a symmetric function of the bending coordinates S_{2a} and S_{2b}, the target vibrational functions for exciting these modes can be classified as even or odd functions of these variables. Since our treatment considers only a single $^2A_1$ negative ion surface, which is also completely symmetric about the initial linear geometry with respect to bending, there is nothing in the dynamics that can cause the initial wave packet to evolve in a way that breaks this symmetry. Consequently, only cross sections corresponding to excitation of an even number of bending quanta are nonzero with this model. This is simply a reflection of the fact that the single-electronic-state model used here does not allow for coupling of the azimuthal angular momentum of the scattered electron and the vibrational angular momentum of the molecule. We shall return to this point in the discussion. Another point concerns the representation of the target vibrational wave functions. The existence

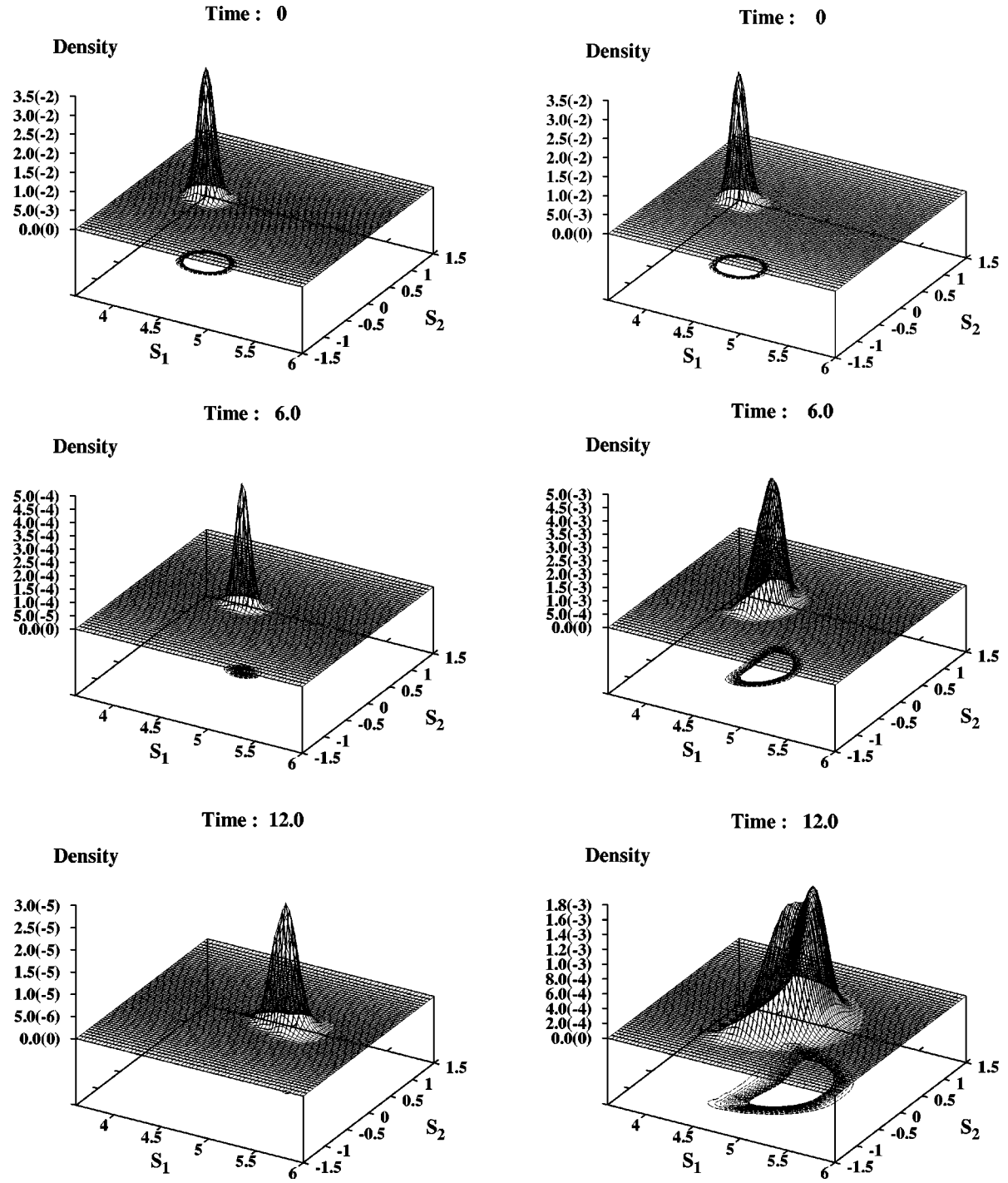

FIG. 8. Probability density from wave packets at three times during propagation: Left column, *ab initio* width function; right column, width decreasing with increasing bending angle. All quantities are in atomic units. Numbers in parentheses on vertical axes indicate power of 10, i.e., $5(-4)=5\times10^{-4}$.

of an accidental near degeneracy, or Fermi resonance, between the (1,0,0) and (0,2,0) vibrational levels of CO_2^- is well known. Because of this degeneracy and the fact that the two states have the same symmetry, the normal mode description of the vibrational wave functions is not valid, as the true wave functions of this ''Fermi dyad'' are almost 50-50 mixtures of zeroth-order symmetric-stretch and bend states [33]. This near degenerate grouping of states extends to higher polyads—for example, the (2,0,0), (1,2,0), (0,4,0) triad—making it impossible to talk about a series of pure symmetric-stretch or bend states. If one uses product wave functions for the vibrational target states as we have done here, then it is important to bear in mind that the appropriate linear combinations of these states (and, consequently, coherent combinations of the corresponding excitation *amplitudes*) must be used to describe the true physical states.

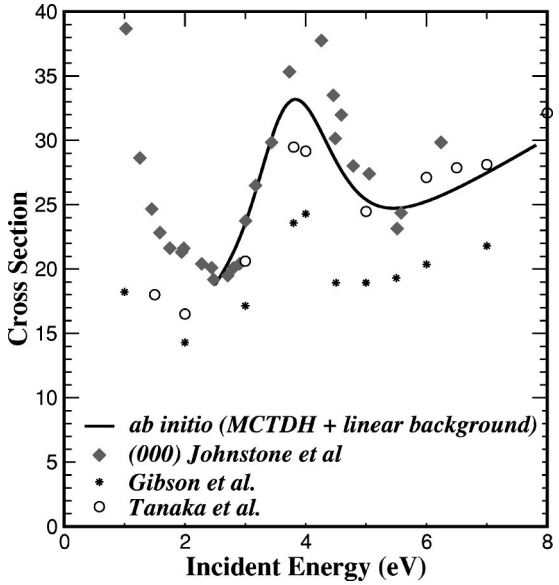

FIG. 9. Integrated vibrationally elastic cross sections, in units of a_0^2, for $e^- + CO_2$. 3D boomerang + calculated background cross sections from Rescigno *et al.* [15] compared with experimental results of Tanaka *et al.* [36], Gibson *et al.* [37], and Johnstone *et al.* [20]. Differential cross sections of Johnstone *et al.* at 20° were multiplied by a factor of 20.

Figure 10 shows cross sections for the ''pure'' (0,0,0) $\rightarrow$(1,0,0) symmetric-stretch excitation calculated in 1D, 2D, and 3D. The damping of the interference structure in the multidimensional treatments is again strikingly evident, although the envelope of the cross section is rather insensitive to the dimensionality of the ion surface. We have also carried out calculations in 3D for a progression of symmetric-stretch excitation cross sections, which are shown in Fig. 11. There is evidently no shift in the peak position as the level of excitation increases, but one can see some weak interference structure beginning with (4,0,0) that gradually increases

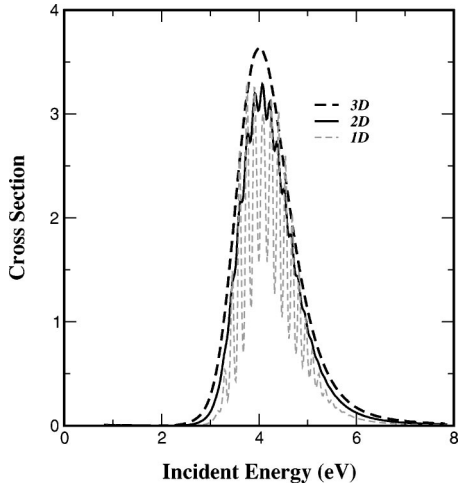

FIG. 10. Integrated vibrationally inelastic cross sections, in units of a_0^2, for $e^- + CO_2$. ''Pure'' symmetric-stretch (see text) (0,0,0) $\rightarrow$(1,0,0) cross sections from 1D, 2D, and 3D boomerang calculations.

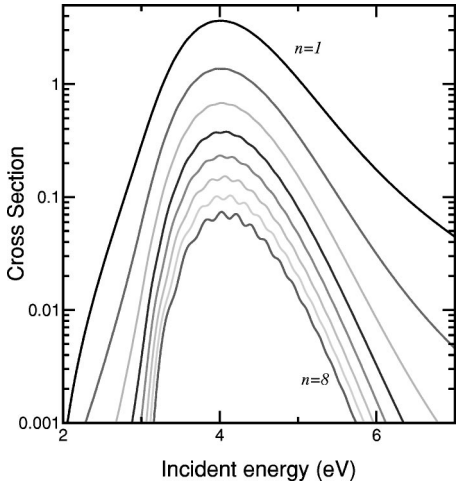

FIG. 11. Integrated vibrationally inelastic cross sections, in units of a_0^2, for $e^- + CO_2$. ''Pure'' symmetric stretch progression (see text) (0,0,0)$\rightarrow$(n,0,0) cross sections from 3D boomerang calculations.

with excitation. This latter effect results from the fact that the wave functions for the higher vibrational levels extend closer and closer to the outer classical turning point and thus overlap more effectively with the wave packet before it decays.

Figure 12 shows the pure bend (0,0,0)$\rightarrow$(0,2,0) excitation cross sections from the MCTDH calculations in 2D and 3D. The 2D results (which have been multiplied by 2 for consistency with the full 3D results) again show weak interference structure which is absent in the 3D calculations. In comparing these cross sections with those for exciting the symmetric stretch modes, one notes that there is a shift in the peak position of almost 1 eV and a significant difference in the overall shape. Another striking difference is that the bending excitation cross sections appear to have a significant background component that rises with decreasing collision energy. We must emphasize that these calculations capture only the resonance component of the excitation cross sec-

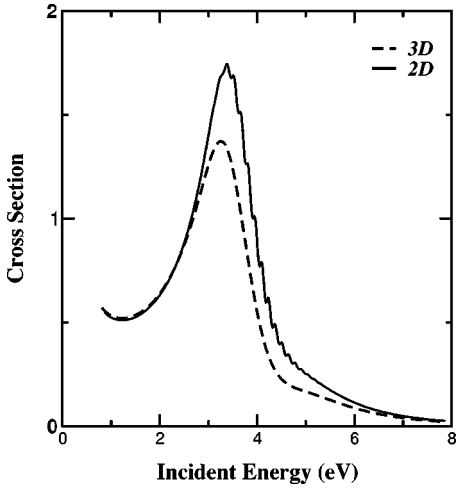

FIG. 12. Integrated vibrationally inelastic cross sections, in units of a_0^2, for $e^- + CO_2$. ''Pure'' bend (see text) (0,0,0)$\rightarrow$(0,2,0) cross sections from 2D and 3D boomerang calculations.

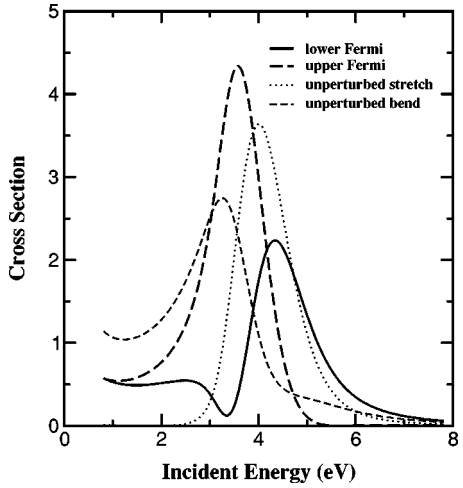

FIG. 13. The effect of Fermi resonance on vibrationally inelastic cross sections, in units of a_0^2, for $e^- + CO_2^-$: comparison of vibrational excitation cross sections computed using unperturbed and perturbed (Fermi dyad) representations of the vibrational wave functions.

tions, so we cannot attribute the ''background'' to the virtual state mechanism that is responsible for the low-energy behavior in the total elastic cross section. The behavior of the $(0,0,0)\rightarrow(0,2,0)$ excitation cross sections is solely a result of the topology of the width surface.

The strong mixing of the two normal modes by the Fermi resonance requires that the computed excitation amplitudes, which refer to the unperturbed target states, be appropriately combined with the correct mixing coefficients. We write the physical vibrational wave functions as

$$\eta_I = a\,\eta_{100} - b\,\eta_{020} \quad \text{(lower Fermi)},$$

$$\eta_{II} = b\,\eta_{100} + a\,\eta_{020} \quad \text{(upper Fermi)}. \tag{3.8}$$

For the coefficients in Eq. (3.8), we used the values $a = 0.763$ and $b = 0.647$ derived by Dennison [39]. Figure 13 compares the excitation cross sections using these perturbed wave functions with those computed using unperturbed normal mode wave functions. The effect is very significant, reflecting the strong mixing of the normal modes in the physical members of the Fermi dyad and the very different ways in which those modes couple to the resonance surface. Figure 14 compares the calculated cross sections with two sets of experimental data. The measurements of Johnstone *et al.* [20], like the elastic results mentioned earlier, were taken at a fixed angle of 20° and were thus scaled by the same factor to compare with our calculated total cross sections. The recently reported measurements of Allan [21], which are also shown in Fig. 14, were taken at a scattering angle of 135°; scaling these data by a factor of 4π gave values that compare well with our calculated results. The *ab initio* results agree rather well with the experimental data, especially in the location and relative magnitude of the peak cross sections, as well as their overall energy dependence. We note that the good relative agreement between the two sets of experimental differential cross section measurements at 20° and 135° indicates that the assumption that the energy and angular dependence of the cross sections are approximately factorable is probably valid here.

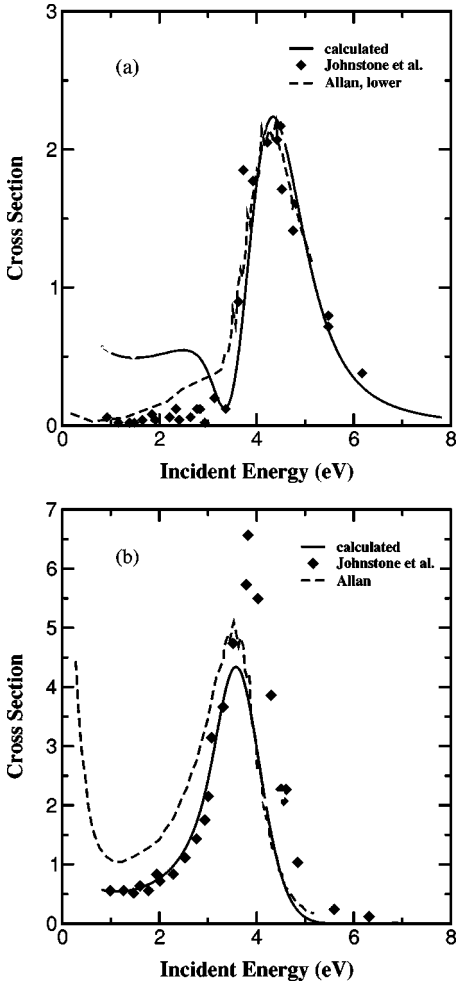

FIG. 14. Comparison of computed cross sections, in units of a_0^2, for excitation of lowest Fermi dyad with experimental results of Johnstone *et al.* [20] and Allan [21]. (a) Lower Fermi level; (b) upper Fermi level.

IV. DISCUSSION

We have attempted to show that the treatment of polyatomic effects in resonant electron-molecule collisions is amenable to a first-principles approach and have used the CO_2 target as an example. We have demonstrated that the interesting topology of the resonance surface demands a realistic multidimensional treatment of the nuclear dynamics. In fact, the strong mixing of the vibrational modes due to Fermi resonance led to effects that cannot even be discussed within the context of a linear model. We are certainly not the first to suggest that polyatomic effects are important in this case. Currell and Comer [19] pointed out the importance of considering both stretching and bending in explaining e-CO_2 vibrational dynamics as early as 1993 and Kazanskii [11,12] has performed model calculations on this problem as well. However, in the absence of accurate fixed-nuclei data for

both linear and nonlinear target geometries, no previous treatments have been able to achieve better than rough qualitative agreement with experiment.

While these results represent an important first step in approaching resonant vibrational excitation in CO_2 completely from first principles, there are still a number of questions to be answered. The unprecedented energy resolution achieved in Allan's measurements [21] makes it clear that the interference structure, although very weak, is present in the excitation cross sections for the lowest Fermi dyad, while our 3D calculations show no structure at all. Another curious difference concerns the energy behavior of the cross sections on the low-energy side of the resonance peak. In both Allan's measurements and those of Johnstone *et al.* [20], only the upper level of the Fermi dyad has a nonzero background, while our calculations show a background for both levels. The reason our calculations show this behavior is clear: the unperturbed symmetric-stretch cross section has no background, so when we take linear combinations of the two amplitudes to form the cross sections for the dyad, the bend amplitude gives a nonzero background for both levels.

There are several effects yet to be investigated. One possibility is that inclusion of asymetric stretch motion would mitigate the dominance of the bending motion on the resonance lifetime and lead to the weak interference structure that is now missing. It is difficult to see, however, how such an effect could cause the background cross section to vanish for only one of the levels of the dyad. Another open question is what effect the $^2B_1$ component of resonance would have on the dynamics. While we have yet to treat this problem in any detail, preliminary investigations indicate that the $^2B_1$ resonance surface has a much weaker dependence on bend than the $^2A_1$ state we have considered here, so including it in the dynamics might well change both the interference structure and the background cross sections. Morever, nonadiabatic coupling between the two resonance surfaces [40] could lead to symmetry breaking effects that would provide a mechanism for resonant excitation of odd levels of the bending modes, which are known to be present [41]. We plan to investigate these problems in future work.

We make a final point in closing. We have discussed the increase in the width of the $^2A_1$ resonance upon bending in terms of symmetry breaking and the admixture of an *s*-wave component into the resonance. The tacit assumption we have made is that the resonance surface is a continuous function of the bend angle and smoothly connects with the region where it becomes electronically bound. We have not discussed how the presence of the dipole moment that accompanies bending impacts this picture. The work of Domcke [22] and others might even call the local complex potential model we have used into question. The quality of the results we have obtained, however, would suggest that we have captured the dominant physical mechanisms responsible for the resonant vibrational excitation of CO_2.

ACKNOWLEDGMENTS

This work was performed under the auspices of the U.S. Department of Energy by the University of California, Lawrence Berkeley, and Lawrence Livermore National Laboratories under Contract Nos. DE-AC03-76SF00098 and W-7405-Eng-48, respectively. The work was supported by the U.S. DOE Office of Basic Energy Science, Division of Chemical Sciences, and computations were carried out at the National Energy Research Scientific Computing Center at Lawrence Berkeley National Laboratory. A.E.O. acknowledges support from the National Science Foundation (Grant No. PHY-99-87877). H.D.M. gratefully acknowledges support through the ''DFG Forschergruppe: Schwellenverhalten, Resonanzen und nichtlokale Wechselwirkungen bei niederenergetischen Streuprozessen.''

[1] *Computational Methods for Electron-Molecule Collisions*, edited by W.M. Huo and F.A. Gianturco (Plenum, New York, 1995).
[2] H. Feshbach, Ann. Phys. (N.Y.) **19**, 287 (1962).
[3] T.F. O'Malley, Phys. Rev. **150**, 14 (1966).
[4] D.T. Birtwistle and A. Herzenberg, J. Phys. B **4**, 53 (1971).
[5] A.U. Hazi, T.N. Rescigno, and M. Kurilla, Phys. Rev. A **23**, 1089 (1981).
[6] T.N. Rescigno, A.E. Orel, and C.W. McCurdy, J. Chem. Phys. **73**, 6347 (1980).
[7] S. Yabushita and C.W. McCurdy, J. Chem. Phys. **83**, 3547 (1985).
[8] U.V. Riss and H.-D. Meyer, J. Phys. B **26**, 4503 (1993).
[9] T. Sommerfeld, F. Tarantelli, H.-D. Meyer, and L.S. Cederbaum, J. Chem. Phys. **112**, 6635 (2000).
[10] A.E. Orel and K.C. Kulander, Phys. Rev. Lett. **71**, 4315 (1993).
[11] A.K. Kazansky and L.Y. Sergeeva, J. Phys. B **27**, 3217 (1994).
[12] A.K. Kazansky, Opt. Spectrosc. **87**, 840 (1999).
[13] M.A. Morrison, N.F. Lane, and L.A. Collins, Phys. Rev. A **15**, 2186 (1977).
[14] L.A. Morgan, Phys. Rev. Lett. **80**, 1873 (1998).
[15] T.N. Rescigno, D.A. Byrum, W.A. Isaacs, and C.W. McCurdy, Phys. Rev. A **60**, 2186 (1999).
[16] C.-H. Lee, C. Winstead, and V. McKoy, J. Chem. Phys. **111**, 5056 (1999).
[17] M.J.W. Bonness and J.B. Hasted, Phys. Lett. **21**, 526 (1966).
[18] I. Cadez, F. Gresteau, M. Tronc, and R.I. Hall, J. Phys. B **10**, 3821 (1977).
[19] F. Currell and J. Comer, J. Phys. B **26**, 2463 (1993).
[20] W.M. Johnstone, P. Akther, and W.R. Newell, J. Phys. B **28**, 743 (1995).
[21] M. Allan, Phys. Rev. Lett. **87**, 033201 (2001).
[22] W. Domcke, Phys. Rep. **208**, 97 (1991).
[23] A.U. Hazi, A.E. Orel, and T.N. Rescigno, Phys. Rev. Lett. **46**, 918 (1981).
[24] C. Mundel, M. Berman, and W. Domcke, Phys. Rev. A **32**, 181 (1985).
[25] G.A. Gallup, Y. Xu, and I.I. Fabrikant, Phys. Rev. A **57**, 2596 (1998).
[26] C.W. McCurdy and J.L. Turner, J. Chem. Phys. **78**, 6773 (1983).

[27] M.H. Beck, A. Jäckle, G.A. Worth, and H.-D. Meyer, Phys. Rep. **324**, 1 (2000).
[28] J.C. Light, in *Time-Dependent Quantum Molecular Dynamics*, edited by J. Broechkove and L. Lathouwers (Plenum, New York, 1992).
[29] G. Worth, H.-D. Meyer, and L.S. Cederbaum, J. Chem. Phys. **109**, 3518 (1998).
[30] A. Raab, G. Worth, H.-D. Meyer, and L.S. Cederbaum, J. Chem. Phys. **110**, 936 (1999).
[31] H. Wang, J. Chem. Phys. **113**, 994 (2000).
[32] A.U. Hazi, Phys. Rev. A **19**, 920 (1979).
[33] G. Herzberg, *Molecular Spectra and Molecular Structure II. Infrared and Raman Spectra of Polyatomic Molecules* (Van Nostrand Reinhold, New York, 1945).
[34] D.G. Hopper, Chem. Phys. **53**, 85 (1980).
[35] G.L. Gutsev, R.J. Bartlett, and R.N. Compton, J. Chem. Phys. **108**, 6756 (1998).
[36] H. Tanaka, T. Ishikawa, T. Masai, T. Sagara, L. Boesten, M. Takekawa, Y. Itikawa, and M. Kimura, Phys. Rev. A **57**, 1798 (1998).
[37] J.C. Gibson, M.A. Green, K.W. Trantham, S.J. Buckman, P.J.O. Teubner, and M.J. Brunger, J. Phys. B **32**, 213 (1999).
[38] L. Dube and A. Herzenberg, Phys. Rev. A **20**, 194 (1979).
[39] D.M. Dennison, Rev. Mod. Phys. **12**, 175 (1940).
[40] H. Estrada, L.S. Cederbaum, and W. Domcke, J. Chem. Phys. **84**, 152 (1986).
[41] M. Allan (private communication).